

PARAMETERS SELECTION FOR THE PRODUCTION OF FULLY DENSE METALS PROCESSED BY SELECTIVE LASER MELTING

M. Ben Slama¹, S. Chatti^{1*}, L. Kolsi^{2,3}

¹Laboratory of Mechanical Engineering, National Engineering School of Monastir, University of Monastir, Rue Ibn El Jazzar, 5000 Monastir, Tunisia

²Department of Mechanical Engineering, College of Engineering, University of Ha'il, Ha'il City 81451, Saudi Arabia

³Laboratory of Metrology and Energy Systems, Department of Energy Engineering, University of Monastir, 5000 Monastir, Tunisia

*Corresponding author's e-mail address: sami.chatti@udo.edu

ABSTRACT

Selective laser melting (SLM) presents significant assets for both industrial and academic fields. However, the process parameters selection is yet challenging. It presents tens of parameters to be carefully selected, including laser power and speed, bed thickness, hatching space, and other parameters, for the manufacturing of parts with high density. This paper provides a deeper understanding of the processing parameters' effect on the evolution of the product's density. A series of numerical simulations of porosity is achieved on Ansys Additive© software and it shows the evolution of the relative density at different laser powers and scan speeds. Numerical results show that low laser power and accelerated scan lead to the generation of a small melt pool, and consequently low density. In the opposite case, at high power and slow scan, the created melt pool is wide enough to avoid porosity and generate fully dense products. The product density is proportionally related to the melt pool size. Hence, it could be estimated through the correlation with the melt pool width, which enables the perfect selection of the hatching space for the selected set of parameters.

KEYWORDS: Additive Manufacturing, Selective Laser Melting, porosity, processing parameters, numerical analysis.

1. INTRODUCTION

Selective laser melting (SLM) is a powder-based additive manufacturing (AM) process allowing the 3D printing of metals. This innovative technology produces metallic products, layer by layer, in a single step and with no specific tooling [10]. In addition to its potential in the freedom of design, SLM produces parts with high surface finish and improved mechanical properties [5]. Furthermore, through the adjustment of the processing parameters, the product density could be controlled. In fact, some applications in the medical and dental fields require a porous structure to simulate human bone behaviour [14]. Nevertheless, other applications, specifically with mechanical performance, require fully dense structures [15]. Herzog et al. [8] announced that enhancing the part density is considered the main objective in AM process optimization. The authors stated in their review that the part density should be higher than 99.5% in order to be classified as dense material. Vast literature revealed the relationship

between product density and its mechanical properties. Baufeld et al. stated the value of 6% for porosity to avoid the gas caption. Otherwise, exceeding this limit, the material's mechanical properties remarkably decrease [2]. Fera et al. showed that the mechanical properties of materials processed by SLM are comparable to those traditionally produced. An exception of the materials presenting high porosity was highlighted [4]. Maskery et al. explained the deterioration of the mechanical properties by the fact that residual porosity in the product facilitates the propagation of cracks that influences its mechanical characteristics [12].

These findings point to the importance of the production of parts with high density for the enhancement of their mechanical properties. Thus, SLM processing parameters have to be carefully selected, which is considered to be a challenging task. In fact, SLM is considered a complex process that simultaneously clusters several complex phenomena at a multiscale. Therefore, it is not evident to control the

quality of the parts during the process [7]. Furthermore, this technology presents multiple parameters to be perfectly selected, which hardens the responsibility of decision-making during the pre-processing stage. SLM process parameters are related to the laser source, such as the laser power and beam width, to the material, like the powder size and morphology, to the bed thickness, or they may be related to the scanning strategy like the scan speed and hatching space [6]. Each parameter from those previously listed influences the product porosity that needs to be investigated. In most cases, as the printing machine already has fixed parameters (beam width, power, and speed) and the powder-related parameters are dictated by the powder supplier, the powder thickness and hatching space remain to be correctly chosen. As for the powder layer, it is selected in most cases considering the geometrical tolerances and the printing time. On the other hand, the hatching space is preferred in order to prevent unmelted regions regarding the melt pool geometry.

The effect of the processing parameters, mainly the laser power, scan speed, layer thickness, and hatching space, on the density of the products processed by SLM was briefly reported in the literature. Generally, small intervals of these parameters were discussed, therefore their effects on the resulting density were not evident [11, 13]. Furthermore, the correlation between the melt pool dimensions and the product density was not clearly and explicitly described.

In this paper, the porosity and melt pool dimensions of the 316L SS are predicted through a series of numerical investigations developed on Ansys Additive © software. The effect of the scan speed, laser power and hatching space on the product density is discussed. In this study, extended intervals of the laser power and the scanning speeds are considered. The relationship between the melt pool dimensions and the relative density is highlighted, allowing the possibility to predict the density through the depth and width of the melt pool that resulted from a single track. Consequently, a conspicuous method for the processing parameters selection is developed. In section 2 of the paper, a description of the numerical model is detailed and the used equations, as well as the boundary conditions and the model inputs and outputs, are listed. In section 3, the relationship between the melt pool dimensions and the resulting density is discussed. The numerical results related to the melt pool depth and width as well as the product density, are presented in section 4. In this section, the effect of the laser power and the scan speed of the melt pool dimensions and consequently of the relative density, as well as the effect of the hatching space on the density, are discussed. The main results are concluded in section 5.

2. NUMERICAL MODELLING

The numerical simulations are developed through a new module from Ansys© software, the so-called

Ansys Additive©. Porosity analysis is carried out through a thermal model where the heat transfer equation described by equation 1 [9] is used.

$$\rho C \left(\frac{\partial T}{\partial t} + \{v\}^T \{L\} T \right) + \{L\}^T \{q\} = \ddot{q} \quad (1)$$

Where ρ , C , T , $\{q\}$, \ddot{q} , $\{L\}$ and $\{v\}$ represent the material density, the specific heat, the temperature, the heat flux vector, the heat generation rate per unit volume, an operator vector and the velocity vector for mass transport of heat. For this thermal model, the heat source is considered a simple volumetric Gaussian laser model. The model geometry is cubic with a volume of $(3 \text{ mm})^3$. Thermal boundary conditions of the model are summarized in table 1.

Table 1. Thermal boundary conditions (BC)

Position	Boundary conditions
Upper face	Uniform convection
Base plate	Fixed temperature
Lateral faces	Adiabatic BC

In this study, a particular focus on stainless steel is established for its remarkable properties and its demand in engineering applications. Furthermore, this material is the only available steel in the software database. The used material properties are temperature dependent for the solid state as well as for the liquid state.

The powder layer is modelled as a homogenous solid with a conversion coefficient between the solid and powder parameters. The model is meshed as a Cartesian grid with a constant size of $15 \mu\text{m}$ in the horizontal directions. In the vertical direction, which is the building direction, the mesh is dynamic and depends on the layer thickness value.

The model's inputs, illustrated in figure 1 and summarized in table 2, are divided into fixed parameters and variable parameters. The fixed parameters are selected like the values mostly reported by literature and according to the software recommendations. As for the variable parameters, their selection is achieved to englobe a large number of combinations. Three values of laser power are selected to perform simulations on relatively low, medium, and high powers. The scan speed is selected to predict the evolution of both the melt pool and density, as the scan accelerates. Therefore, a series of scan speeds are chosen, starting from the slow scan (400 mm/s) to the accelerated scan (2000 mm/s) with steps of 100 mm/s.

3. RELATIONSHIP BETWEEN DENSITY AND MELT POOL SIZE

During SLM, a laser beam selectively fuses powder to the melting temperature. As the powder melts, a melt pool is formed and moved through the scanning line.

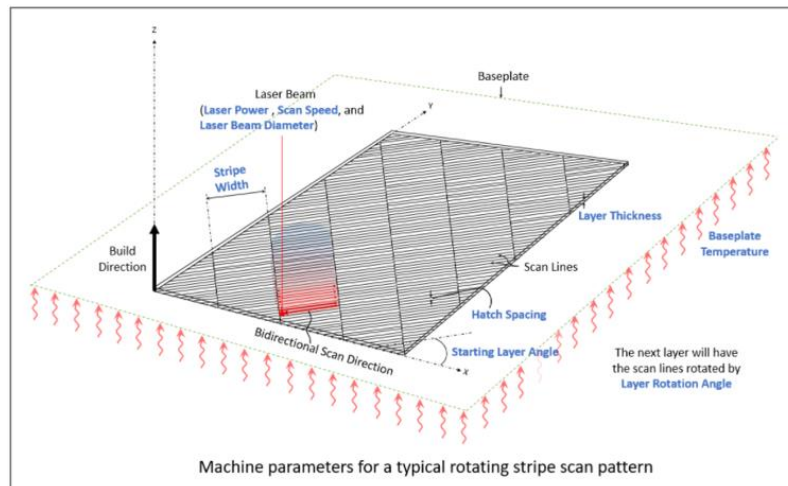


Fig. 1. Schematic illustration of the model inputs [1]

Table 2. Numerical model inputs

	Model inputs	Values
Fixed parameters	Sample dimensions (mm)	3 x 3 x 3
	Base plate temperature (°C)	80
	Laser beam diameter (μm)	100
	Slicing stripe width (mm)	10
	Starting layer angle (°)	57
	Layer rotation angle (°)	67
Variable parameters	Layer thickness (μm)	70
	Hatching space (μm)	100, 150
	Laser power (W)	100, 200, 300
	Scan speed (mm/s)	400-2000 with steps of 100 mm/s

This line is called a single bead or also a weld. The laser scans the proposed surface, according to the scanning strategy, line by line, and is separated by a small distance, the so-called “hatching space”. When the totality of the surface is scanned, the platform moves down by the value of the layer thickness, a new layer of powder is spread, and the scan of the new layer begins.

As an undesirable consequence of both horizontal (in the powder bed plane) and vertical (in the building direction) scans, unmelted regions could occur, as illustrated in figure 2.

The weld’s width will certainly affect the choice of the hatching space. In fact, as the hatching space (H) is higher than the melt pool width (W), an unmelted powder localized between two consecutive lines remains. The overlap distance (H) is directly proportional to the melt pool width (W) (equation 2).

$$Overlap = x \times W \quad (2)$$

Where x is the proportionality factor ($0 < x < 1$). The relationship between the selected hatching space and the melt pool depth is described by equation (3):

$$H = W - Overlap = W \times (1 - x) \quad (3)$$

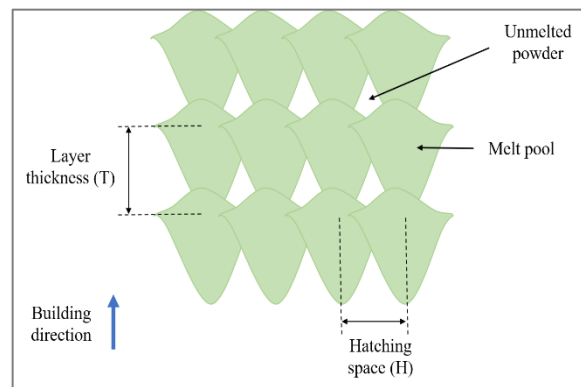


Fig. 2. Schematic illustration of the unmelted powder between the scanned lines

In the opposite case, as the hatching space is lower than the melt pool width, the consecutive welds are overlapped, and no porosity is generated in the horizontal direction. Figure 3 presents a schematic configuration of the two cases where the hatching space is higher and lower than the weld width. This figure illustrates the two possible choices of the hatching space in relationship to the melt pool width. In the first configuration (Fig. 3a), the hatching space (H1) is larger than the melt pool width. In this case, the created weld is too far from the consecutive one and does not fuse with it. Consequently, metallic powder remains between these two tracks. In the opposite configuration (Fig. 3b), the hatching space (H2) is lower than the melt pool depth. In this case, the consecutive tracks fuse together within a so-called distance overlap. Consequently, no powder remains between the consecutive welds. In the vertical direction, the melt pool (MP) depth should exceed 1.5 times the layer thickness in order to avoid the Lack of Fusion (LOF) between two consecutive layers. Otherwise, unmelted powder remains between layers.

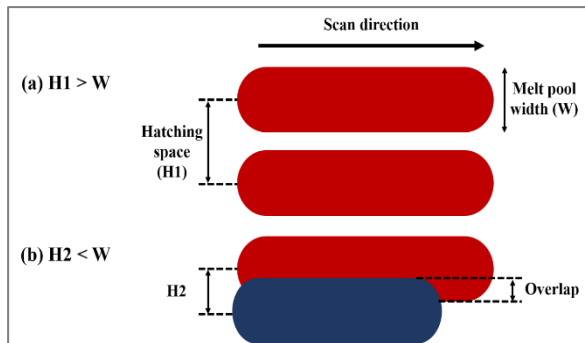


Fig. 3. Schematic illustration of the relationship between the hatching space and the MP width

4. RESULTS AND DISCUSSION

4.1. Melt Pool Size

The achieved simulations allowed the traceability of the melt pool size (depth and width) as the scan speed increased at different values of laser power. Figures 4 (a) and (b) present the melt pool depth and width for the concerned combinations.

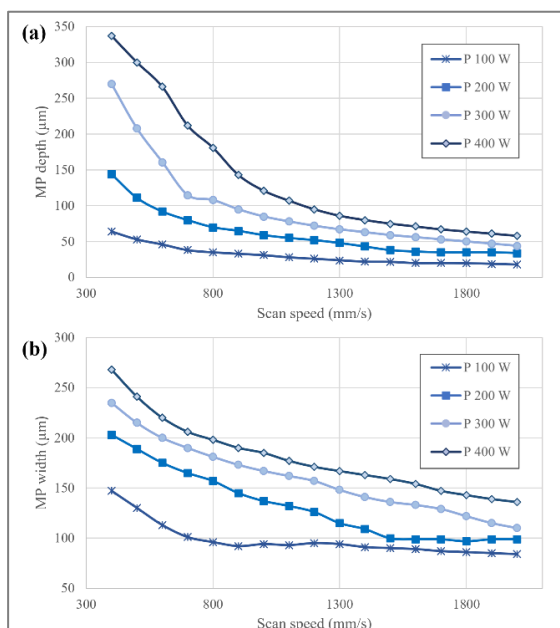


Fig. 4. Melt pool evolution at various scan speeds for different values of laser power: a) depth; b) width

Obviously, for all values of the laser power, both melt pool depth and width decrease as the scan accelerates. Such observation is consistent and in accordance with the physical phenomena. In fact, at an accelerated scan, there is not enough time to form a wide melt pool and to penetrate in depth as well. On the contrary, at a low scan speed, a deeper and wider melt pool is formed. The effect of the laser power is observed mainly for low values of the scan speed. For low powers, the melt pool depth is about 50 μm , which is too small (smaller than the layer thickness of

70 μm) to fuse with the substrate. As the laser power increases, the melt pool depth increases, which is anticipated. In fact, more energy is absorbed by the metallic powder when the laser power is higher. Consequently, a deeper melt pool is generated. The highest power (400 W) generates a deep melt pool of about 350 μm , which equals 5 times the layer thickness. Despite the fact that this melt pool ensures the prevention of the LOF, it could generate another type of defect.

As for the melt pool width, the same evolution is observed, except for its moderated increase as the laser power increases.

4.2. Relative Density

The relative density that results from using the selected combinations of laser power, scan speed and a fixed hatching space of 100 μm , is presented in figure 5.

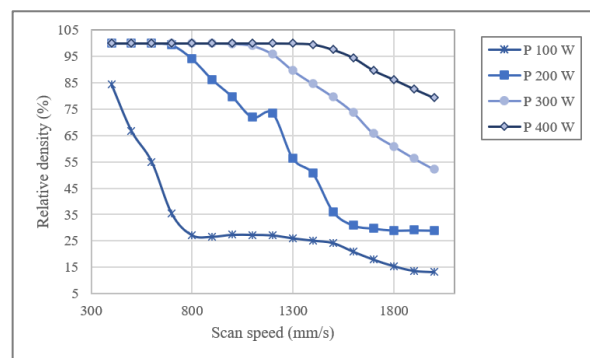


Fig. 5. Relative density for several combinations of laser power and scan speed for a constant hatching space (100 μm)

At a constant hatching space (100 μm), the relative density decreases as the scan speed increases for all series of laser powers. For the lowest power (100 W), the maximum density is about 85%, which is too low to be accepted. As the scan accelerates, the relative density sharply decreases, and then it almost remains constant beginning from 800 mm/s, which is similar to the melt pool width evolution for the same power value. This low density is attributed to the small melt pool generated at this power.

As the laser power increases, the relative density increases and reaches the full density for high powers and low scan speeds.

This finding favourably correlates with the melt pool size evolution. Hence, for high powers and low scan speeds, a large and deep melt pool is created which prevents both horizontal and vertical lack of fusion. In this case, no unmelted powder remains between welds, and no porosity is generated. On the other hand, when the scan speed increases the melt pool size decreases, and porosity is formed. The low density is conceivably generated due to a lack of fusion between two consecutive horizontal welds. In

fact, this defect appears if the hatching space is too large to create a sufficient overlap between two consecutive welds, as illustrated in figure 3 (a). In this case, an overlapping distance of 37.5% of the melt pool ($x=0.375$) is proposed. Thus, as the hatching space is fixed at 100 μm , the laser power-scan speed combination that generates a melt pool under 160 μm will present porosity (relative density < 100%).

In order to study the effect of the hatching space on the relative density, two values are investigated (100 μm and 150 μm). The evolution of the relative density as the scan speed accelerates at a constant power of 300 W (arbitrarily chosen) is presented in figure 6. Results show that the relative density generated in low scan speed is 100%, representing full density, in both cases. However, the density generated by higher hatching space drops to lower values of scan speed. This result is already anticipated by the relationship between the hatching space and the melt pool width. In fact, when the hatching space equals 100 μm , fully dense products are generated as the melt pool width is over 160 μm . As for the new value of hatching space (150 μm), porosity begins to appear at higher values of the melt pool width. Below 100%, the relative density decreases, as the scan accelerates for both cases. It can be remarked that higher hatching space leads to lower density.

Since the relative density depends on laser power, scan speed, thickness, and hatching space, this can be expressed by the volumetric energy density. This energy is the ratio of the laser power to the product of the speed, thickness, and hatching space [16], as described in equation 4.

$$VED = \frac{P}{S.T.H} \tag{4}$$

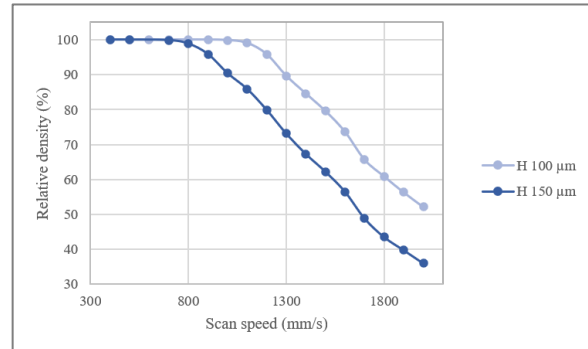


Fig. 6. Relative density evolution for different scan speeds at a constant laser power of 300 W and different values of hatching space

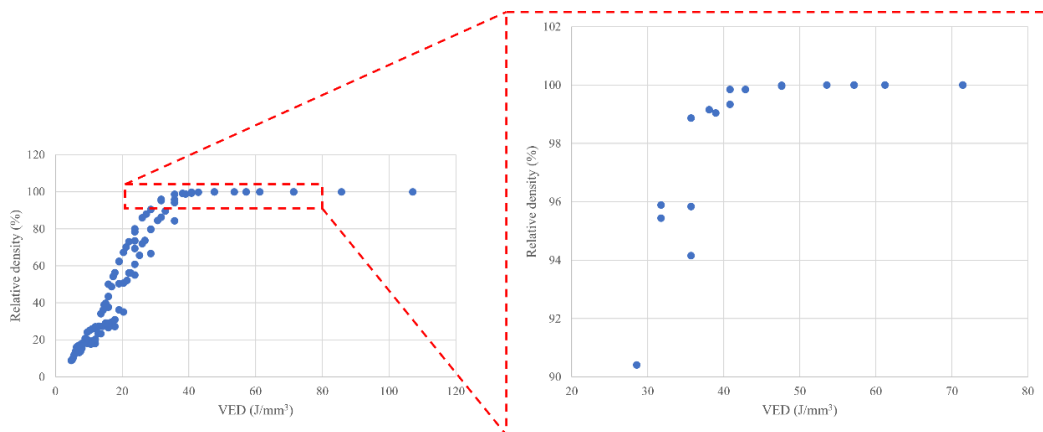


Fig. 7. Relative density as function of the volumetric energy density for a constant hatching space

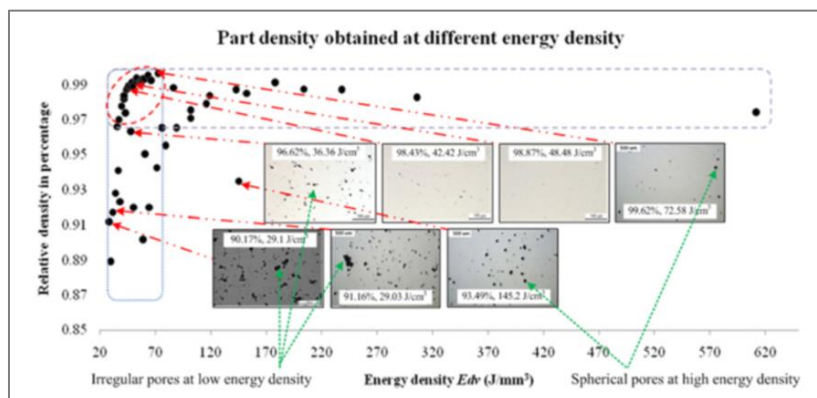


Fig. 8. Part density obtained at different energy densities showing the relationship between the resulting porosity and the input energy density [3]

Figure 7 illustrates the evolution of the relative density in terms of volumetric energy density (VED). Results show that the energy density proportionally increases with the volumetric energy density. Low energy density displays low laser power and high scan speed, presenting the combinations that generate a small melt pool. On the other hand, high energy density is generated with high laser power and slow scan speed, which are favourable conditions for the generation of large melt pools. This proves the previously mentioned relationship between the melt pool size and the volumetric energy density.

Relatively high densities (> 90%) are highlighted in the red dashed zone. This zoomed part of the curve depicts that the energy values beyond 35 J/mm³ are the most effective (generating porosity higher than 95%). These results correlate well with experimental findings and are presented in figure 8. Chen et al. also proposed that the effective energy zone (E²O) covers values ranging between 35 and 70 J/mm³ [3].

5. CONCLUSIONS

Selective laser melting (SLM) is known for its potential in producing superior quality parts. However, the product's mechanical properties are remarkably affected by the residual porosity. Thus, the printed parts should have a density of over 99.5%. Nevertheless, in order to control the residual density, the effect of the processing parameters has to be deeply understood.

In this study, an investigation of the effect of the laser power and the scan speed on the melt pool size, accordingly to the resulting density, has been made. Hence, the relationship between the relative density and the melt pool depth and width was established. Furthermore, full density could be predicted through both melt pool width and hatching space, through a proportionality equation. Numerical simulations performed by Ansys Additive © software were carried out. In light of this study, the following conclusions can be drawn:

- as the laser power increases, the melt pool depth and width increase too due to the rising input energy absorbed by the metallic powder.
- as the laser scan accelerates, the time required for the absorption of the input energy by the powder bed decreases, leading to a decrease in the melt pool dimensions.
- the same evolution of the melt pool size is observed for the product's relative density.
- at a slow scan, the density reached the maximum value of 100% (fully dense product) and then decreased as the scan speed increased and as the laser power decreased.
- the product density could be estimated from the melt pool width through the selected hatching space.

On the other hand, high laser power and low scan speed lead to a large melt pool and a high density. As for the hatching space, it has an inversely proportional

relation with the relative density. To combine all these processing parameters (laser power, scan speed, hatching space and layer thickness), the evolution of the relative density in terms of volumetric energy density was investigated. An effective zone for the generation of fully dense material is highlighted. Results were in accordance with the experimental results reported by the literature.

REFERENCES

- [1]. *** Ansys, *Additive User's Guide (Print and Science)*, no. January 2021.
- [2]. **Baufeld B., Brandl E., Van der Biest O.**, *Wire based additive layer manufacturing: Comparison of microstructure and mechanical properties of Ti-6Al-4V components fabricated by laser-beam deposition and shaped metal deposition*, J Mater Process Technol, vol. 211, no. 6, pp. 1146–1158, 2011, doi: 10.1016/j.jmatprotec.2011.01.018.
- [3]. **Chen T.**, *Influence of Energy Density on Energy Demand and Porosity of 316L Stainless Steel Fabricated by Selective Laser Melting*, International journal of precision engineering and manufacturing green technology, vol. 5, no. 1, pp. 55–82, 2018.
- [4]. **Fera M., Fruggiero F., Lambiase A., Macchiaroli M.**, *State of the art of additive manufacturing: Review for tolerances, mechanical resistance and production costs*, Cogent Eng, vol. 3, no. 1, p. 1261503, 2016, doi: 10.1080/23311916.2016.1261503.
- [5]. **Gu D., et al.**, *Densification behavior, microstructure evolution, and wear performance of selective laser melting processed commercially pure titanium*, Acta Mater, vol. 60, no. 9, pp. 3849–3860, May 2012, doi: 10.1016/j.actamat.2012.04.006.
- [6]. **Hassine N., Chatti S., Ben Slama M., Kolsi L.**, "Sensitivity of Melt Pool Dimensions and Keyhole to Laser Beam Diameter," Ann. "Dunarea Jos" Univ. Galati, Fascicle XII, Weld. Equip. Technol., vol. 32, pp. 30–36, 2021, doi: 10.35219/awet.2021.04.
- [7]. **Heeling T., Cloots M., Wegener K.**, *Melt pool simulation for the evaluation of process parameters in selective laser melting*, Addit Manuf, vol. 14, pp. 116–125, 2017, doi: 10.1016/j.addma.2017.02.003.
- [8]. **Herzog D., Seyda V., Wycisk E., Emmelmann C.**, *Additive manufacturing of metals*, Acta Mater, vol. 117, pp. 371–392, 2016, doi: 10.1016/j.actamat.2016.07.019.
- [9]. **Johnson L. et al.**, *Assessing printability maps in additive manufacturing of metal alloys*, Acta Mater, vol. 176, pp. 199–210, 2019, doi: 10.1016/j.actamat.2019.07.005.
- [10]. **Luo Z. and Zhao Y.**, *Efficient thermal finite element modeling of selective laser melting of Inconel 718*, Comput Mech, vol. 65, no. 3, pp. 763–787, 2020, doi: 10.1007/s00466-019-01794-0.
- [11]. **Maamoun. A. H., Xue. Y. F., Elbestawi. M. A., and Veldhuis. S. C.**, "Effect of selective laser melting process parameters on the quality of alloy parts: Powder characterization, density, surface roughness, and dimensional accuracy," Materials (Basel), vol. 11, no. 12, 2018, doi: 10.3390/ma11122343.
- [12]. **Maskery I. et al.**, *Quantification and characterisation of porosity in selectively laser melted Al-Si10-Mg using X-ray computed tomography*, Mater Charact, vol. 111, pp. 193–204, 2016, doi: 10.1016/j.matchar.2015.12.001.
- [13]. **Read. N., Wang. W., Essa. V., and Attallah. M.**, "Selective laser melting of AlSi10Mg alloy: Process optimisation and mechanical properties development," Mater. Des., vol. 65, pp. 417–424, 2015, doi: 10.1016/j.matdes.2014.09.044.
- [14]. **Ruidi L., Jinhui L., Yusheng S., Mingzhang D.**, *316L Stainless Steel with Gradient Porosity Fabricated by Selective Laser Melting*, J Mater Eng Perform, vol. 19, no. 5, pp. 666–671, 2009.
- [15]. **Shipley H. et al.**, *Optimisation of process parameters to address fundamental challenges during selective laser melting of Ti-6Al-4V: A review*, Int J Mach Tools Manuf, vol. 128, pp. 1–20, 2018, doi: 10.1016/j.ijmactools.2018.01.003.
- [16]. **Sinico M., Witvrouw A., and Dewulf W.**, *Influence of the particle size distribution on surface quality of Maraging 300 parts produced by Laser Powder Bed Fusion*, Proceedings of the Special Interest Group meeting on Advancing Precision in Additive Manufacturing, no. September, pp. 31–34, 2019, [Online].